016
WING–ROTOR INTERACTIONS ON A 1/4–SCALE TILTROTOR HALF–MODEL

G. Droandi*, G. Gibertini*, M. Lanz*, G. Campanardi*, D. Grassi*, S. Garbaccio*

*Dipartimento di Scienze e Tecnologie Aerospaziali – Politecnico di Milano
Campus Bovisa, Via La Masa 34, 20156 Milano – Italy
e–mail: giovanni.droandi@polimi.it

Keywords: Tiltrotor, Aerodynamic, Rotor, Experimental model, PIV measurements.

Abstract

In a tiltrotor aircraft, the aerodynamic interaction between wing and rotors can have a negative influence on the hovering performance and on the lifting capability. In 2011, a research activity has been started at Dipartimento di Scienze e Tecnologie Aerospaziali at Politecnico of Milano to study from both an experimental and numerical point of view the aerodynamic interference between wing and rotor on a tiltwing aircraft. A 0.25 scale model, based on the aircraft geometry defined at the very beginning of this activity, has been manufactured in–house and the experimental test rig represents only one half–wing and the corresponding rotor and nacelle. The rotor performance were evaluated in terms of figure of merit both for the isolated rotor and for the half–model configurations. Two different wing configurations (untilted and tilted) were tested to understand how the airframe affects the rotor performance. The forces generated on wing by the rotor wake were measured for a wide range of thrust coefficients for both wing configuration. Particle–image velocimetry technique was used to acquire two–dimensional images of the flow field close to the tilted part of the wing.

1 Introduction

The hovering performance and the lifting capability of a tiltrotor aircraft are mainly affected by the aerodynamic interaction between wing and rotors. In helicopter mode, the rotor wake strikes on the upper surface of the wing and generates a three–dimensional flow producing competing aerodynamic interactions that are responsible for loss of rotor performance and wing download (see Ref. [1], [2]). The rotor wake impinging on the wing surface creates a download that is approximately $10\% - 15\%$ of the rotor thrust (see Ref. [3]) and negatively affects the rotor performance as the flow blowing from the rotor over the wing is re–absorbed by the rotor itself (see Ref. [4]). Anyway, to have acceptable hover performance, existing tiltrotors (XV–15, V–22 Ospray and BA609) have large rotors that develop high aerodynamic interference in terms of wing–rotor (see Ref. [5]) and rotor–rotor (see Ref. [6]) interaction in helicopter mode and prevent the take–off and landing in aeroplane mode. Furthermore, the large diameter of the rotors gives some limitations in terms of the performance in aeroplane mode. A possible solution to improve the aircraft performance in aeroplane mode is to reduce the rotor diameter and change considerably the blade shape. This solution leads to the tiltwing concept, that is a non conventional tiltrotor configuration in which the basic idea is to tilt the external part of the wing (the part inside the rotor slipstream) to reduce the download effect (less than 1%, see Ref. [7]) and to preserve good performance in helicopter mode. Moreover, the reduction of the rotor diameter allows for horizontal take–off and landing, improves the performance in aeroplane mode increasing the propulsive efficiency of the propeller, and positively affects the width of the conversion corridor. Recently, the tiltwing concept has been adopted inside the framework of the European project ERICA (Enhanced Rotorcraft Innovative Concept Achievement) (see Ref. [8]). During last 10 years, ERICA has been the subject of several studies and research projects (see Ref. [9], [10]) but many fundamental aspects relating to the aerodynamic interaction between wing and rotor in this kind of configuration still have to be investigated more in depth.

In 2011, a research activity has been started at Dipartimento di Scienze e Tecnologie Aerospaziali (DAST) of Politecnico of Milano to study the aerodynamic interference between wing and rotor on a tiltwing aircraft. In particular, an aircraft of the same kind of ERICA has been defined and the operating flight conditions and the geometrical dimensions of the full scale aircraft have been chosen by means of statistical approach (see. Ref. [7]). A half–model configuration has been selected for both experimental and numerical studies. Numerical simulations have been used to get a first insight in the main phenomena associated with aerodynamic interference between wing and rotor, and numerical results have also been used to help the design and the development of the experimental test rig of the 0.25 scale tiltwing half–model.

The subject of the present paper is about the first experimental campaign on the 0.25 scale tiltwing half–model. In the first part of the paper the experimental test rig for hover tests is described. In the second part, the experimental campaign is described and the experimental results are reported. The aerodynamic influence of the rotor on the wing has been evaluated for two wing configurations and the tilted configuration has been compared to the untilted one; measures have been performed with and without the image plane. The Figure of Merit (FM) has been computed for the half–model in several configurations and it has been compared with the FM of the isolated rotor. A comparison between the isolated rotor performance and CFD calculations is also reported. Particle–image velocimetry (PIV) system developed in–house (see Ref. [11]) has been used to acquire two–dimensional images of the flow field under the rotor in a vertical plane, parallel to the chord of the tilted part of the wing.

2 Experimental test rig

The aircraft model represents only one half–wing and the corresponding rotor and nacelle while the aircraft fuselage is not included in the model so that the wing root lies on the aircraft symmetry plane. Numerical calculations have been used to help the design of the experimental test rig as, for example, the definition of the tilt section location on the half–wing and the design of the shape of the rotor blades (see Ref. [7]). The 0.25 scale tiltwing half–model consisted of three main components that are the rotor system, the half–wing and an image plane,

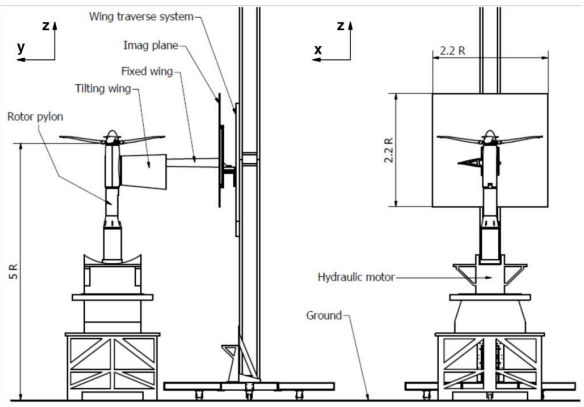

Figure 1: Test rig setup.

Figure 2: Experimental test rig.

r/R	c/R	θ [deg]	$\Delta x/R$	Airfoil
0.216	0.131	9.061	0.000	NACA 0030
0.270	0.133	8.351	0.000	NACA 0020
0.324	0.144	8.324	0.000	NACA 23014
0.487	0.168	5.217	0.003	VR–5
0.649	0.179	-0.005	0.017	OA–213
0.757	0.155	-2.265	0.025	VR–7
0.865	0.154	-2.849	-0.003	VR–5
0.946	0.131	-3.540	-0.046	RC–510
1.000	0.108	-4.759	-0.077	RC–510

Table 1: Geometric characteristics of the blade.

Wing airfoil section	NACA 64A221
Wing root chord	0.750 m
Wing tilt chord	0.625 m
Wing tip chord	0.520 m
Fixed–wing span	0.933 m
Rotating–wing span	0.792 m
Wing twist	0.0 deg
Wing dihedral	0.0 deg
Wing sweep	0.0 deg

Table 2: Geometric characteristics of the wing.

as shown in Figure 1 and 2. The rotor was powered by an hydraulic motor (maximum power 16 kW at 3000 rpm) and the hub was mounted on a rigid pylon located over the motor. The nominal rotational speed of the rotor was 1120 rpm. The tip Mach number was 0.32 which correspond to 1/2 the tip Mach number of full scale aircraft at design point in hover (see Ref. [7]). The rotor had four swept blades with non–linear twist and chord distributions with a thrust weighted solidity $\sigma = 0.192$ (Table 1 summarizes the blade geometry). The rotor radius (R) was 0.925 m and it was placed at an height of 5 R from the ground. The thrust given by the rotor has been measured by a six–component strain gauge balance located under the rotor hub while the torque has been measured by an in–house instrumented holed shaft directly linked to the rotor hub shaft. Under the instrumented shaft, a flexible joint has been used to avoid the transfer of forces to the lower part of the transmission shaft. The nacelle had an external maximum diameter of 0.27 R and it was not weighed because was mounted on the lower part of the rotor pylon. The nacelle air intake has not been taken into account in this study thus it was not present on the nacelle. The half–wing model was 1.90 R long, where the span of the wing had to be intended from the aircraft symmetry plane (wing root) to the nacelle junction (wing tip). The tilt section was located 1.01 R from the symmetry plane and the external part of the wing can rotate from 0° (untilted configuration) to 90° (tilted configuration). The wing was linearly tapered, untwisted and all sections were aligned with respect to the 25% of the local chord. In Table 2 the wing characteristics are reported. The wing was mounted on a independent traversing system and it was not connected to the nacelle and rotor in order to have a more accurate evaluation of the effects due to the impingement of the rotor wake on the airframe model. Forces and moments on the wing have been measured by a seven–component strain gauge balance located at the wing root. The relative distance between the wing axis and the rotor plane has been changed by moving the wing support on its traversing system. The image plane, placed at the wing root, was 2.2 R high and 2.2 R wide (see Ref. [6]).

The four bladed fully articulated rotor hub mounted on the upper part of the rotor pylon represented a typical helicopter hub. The collective, longitudinal and lateral pitch controls were provided to the blades by three electric actuators acting on the swashplate. Each blade was attached to the rotor hub through the flap, led–lag and pitch hinges located in different positions, as shown in Figure 3. In order to measure directly the pitch, led–lag and

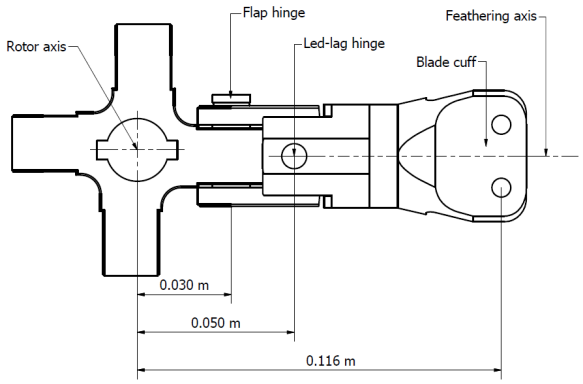

Figure 3: Details of the rotor hub: hinges schema.

flap angles on the rotor hinges, Hall effect sensors have been employed on each blade hinge.

2.1 PIV setup

The PIV setup of the DAST Aerodynamics Laboratory of Politecnico of Milano [12] has been employed to acquire 2D images of the flow field on a vertical plane located under the rotor and close to the rotated part of the wing. The 2D PIV system has been assembled with different components of different brands. In particular, a Dantec Dynamics Nd:YAG double pulsed laser with 200 mJ output energy and a wavelength of 532 nm has been fixed on the pylon support under the rotor. A Pixelfly PCO double shutter CCD camera with a 12 bit, 1280 $\times$ 1024 pixel array has been used to get the image pairs. The camera has been mounted on a single axis traversing system to move the measurement window in vertical direction along the lower surface of the tilted part of the wing. The synchronisation of the two laser pulses with the image pair's exposure has been controlled by a 6 channels Quantum Composer pulse generator. A particle generator PIVpart30 by PIVTEC with Laskin atomizer nozzles has been used for the seeding. The image pairs post-processing has been carried out by PIVview 2C software ([13]) developed by PIVTEC.

3 Test results

The test campaign conducted in the DAST Aerodynamics Laboratory of Politecnico of Milano was divided in two different parts. The first part of the experimental campaign was focused on forces and moments measurements on different model configurations. The rotor performance and the influence of the model airframe on the rotor and vice versa were studied in terms of rotor thrust coefficient (C_T) and power coefficient (C_P), Figure of Merit ($FM = C_T^{3/2}/(C_P\sqrt{2})$) and wing forces. In the last part of experimental campaign 2D PIV measurements were performed on the half–model. No corrections were applied on measurement results.

3.1 Isolated rotor performance

The first tests were conducted on the isolated rotor to characterize the rotor performance at different C_T without airframe interaction. In Figure 4 the FM of the rotor has been reported as function of C_T/σ at the nominal tip Mach number $M_{Tip} = 0.32$. The maximum value of FM is 0.71 and it was obtained for $C_T/\sigma = 0.092$. For the isolated rotor in hover, numerical simulation have been performed with the CFD code ROSITA (ROtorcraft Software ITAly) developed at Politecnico of Milano [14] and [15], based on the solution of the Reynolds Averaged Navier-Stokes (RANS) equations coupled with the one-equation turbulence model of Spalart-Allmaras. Figure 4 shows that CFD calculations well predict the rotor performance for all test conditions. In terms of figure of merit, the maximum difference between numerical and experimental results is 2.3 % at $C_T/\sigma = 0.076$.

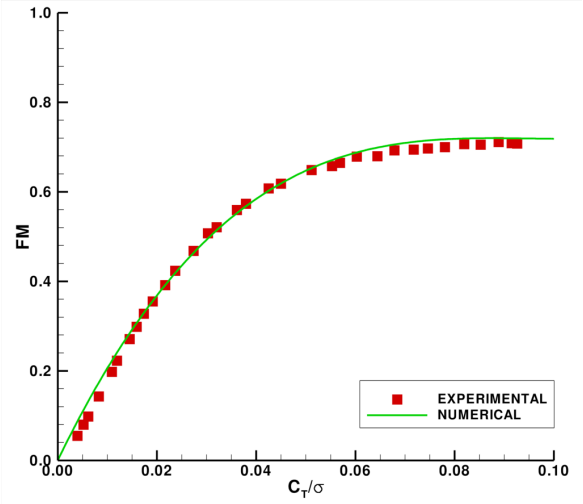

Figure 4: FM as function of C_T/σ for the isolated rotor: experimental results and CFD calculations.

3.2 Effect of wing and image plane on rotor performance

In this part of the experiment, two different wing configurations (untilted and tilted) were tested to understand how the airframe affects the rotor performance. In Figure 5 the rotor performance are reported, while in Figure 6 the rotor FM is presented. In both cases results are compared with the isolated rotor case. In Figure 5 and 6 also the effect of the image plane on the untilted configuration is shown. As already focused by McVeigh

(Ref. [1]) and by Felker and Light (Ref. [3]), the rotor performance with the untilted wing installed below it and without the image plane on the aircraft symmetry plane was greater that the isolated rotor performance. In this case, the partial ground effect given by the wing surface increases the rotor thrust for a given power from a minimum value of 3.4 % at $C_P = 0.0015$ to a maximum value of 5.3 % at $C_P = 0.0023$. From Figure 6, the maximum value of FM is 0.76 at $C_T/\sigma = 0.098$, 6.5 % higher than the isolated rotor case. When the image plane is present, a reduction in the rotor performance with the wing untilted was present if results are compared with the case without the image plane. On the other hand, if results are compared with the isolated rotor performance, an increase in rotor performace is still present. In this second case, the increase in rotor thrust goes from a minimum value of 1.6 % at $C_P = 0.0019$ to a maximum value of 2.5 % at $C_P = 0.0007$. This effect is in contrast with what Felker and Light (Ref. [3]) and McVeigh (Ref. [1]) observed for the XV–15 and V–22 half–models. The reduction in rotor performance measured on that models with the image plane has been justified by the presence of a region close to the symmetry plane and between the rotor and the wing of recirculating flow. Flow visualizations done by Polak et all. (Ref. [6]) and PIV measurements done by Darabi et all. (Ref. [4]) show that for a tiltrotor with large rotor diameter, like the XV–15 and V–22, the fountain flow region is not correctly reproduced when the image plane is employed. In the present case however, since the span of the half–wing is about twice the rotor radius, the negative influence on rotor performance of the fountain flow region due to the image plane is no longer present. Thereby the effect of the image plane on the rotor performance with the wing untilted is an increase in rotor thrust for a given power. The maximum value of FM is 0.73 at $C_T/\sigma = 0.095$, 2.7 % higher than the isolated rotor case.

The second wing configuration tested in this part of the experiment is the tilted configuration and results are shown in Figure 5 and 6. An increase in rotor thrust can be noted if results are compared with isolated rotor performance. As in the previous case, the increase in rotor thrust goes from a minimum value of 1.5 % at $C_P = 0.0019$ to a maximum value of 2.4 % at $C_P = 0.0007$. Therefore, for this configuration no significant differences have been noted in terms of rotor performance when results are compared with the untilted configuration with image plane. Since the rotor wake impinges only on the external part of the wing, that is the part that can be rotated, when the tilted configuration was taken into account, no significant effect due to the image plane was observed. In this case,

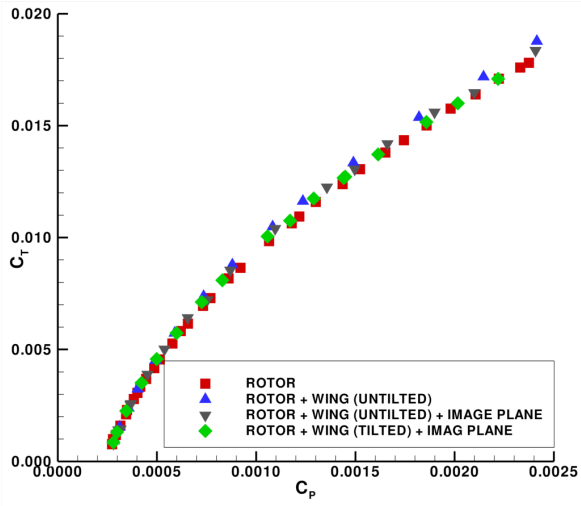

Figure 5: C_T as function of C_P for the half–model tiltrotor.

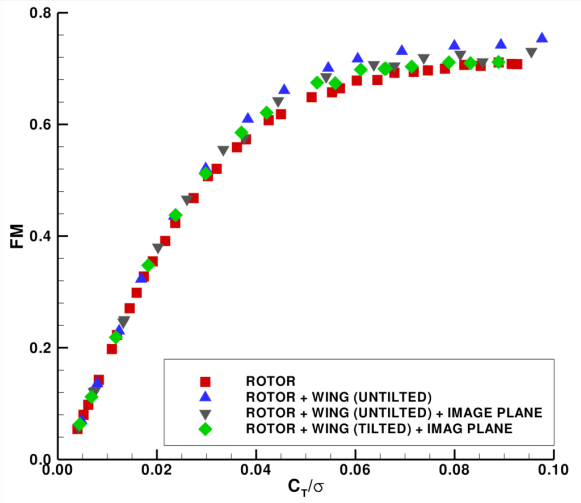

Figure 6: FM as function of C_T/σ for the half–model tiltrotor.

the maximum value of FM is 0.71 at $C_T/\sigma = 0.089$, 2.7 % higher than the isolated rotor case and substantially equal to the untiled wing plus image plane case.

3.3 Effects of the rotor on the wing

The aerodynamic influence given by the rotor wake impinging on the wing has been investigated for two wing configurations (untilted and tilted). As in the previous part, the tests were conducted at a M_{Tip} that is 1/2 the full scale M_{Tip}. Nevertheless, the ratio between the aerodynamic forces acting on the wing and the rotor thrust should be indipendent of the M_{Tip} because the difference between the Reynolds number, based on the tip speed and the wing chord, in the test case ($R_e = 4.4 \times 10^6$)

and in the full scale case ($R_e = 8.8 \times 10^6$) gives no significant effects, as shown by McVeigh (Ref. [1]). In the following, the forces acting on the wing have been expressed in the reference system illustrated in Figure 1.

When the rotor wake strikes on the surface of the wing, an aerodynamic force F_z^w parallel to the z–axis was generated. When the untilted configuration was taken into account the F_z^w on the wing was negative (download) and the highest force/thrust ratio (about 22 %) was obtained at a very low $C_T/\sigma = 0.006$; the force/thrust ratio decreases for higher value of C_T/σ reaching the lower value of 15.6 % at $C_T/\sigma = 0.098$. As shown in Figure 7, the effect of the image plane in this configuration seems to be negligible. A drastic reduction of the vertical force F_z^w acting on the wing was observed on the tilted configuration. Even though the force/thrust ratio is less than 0.8 % for all C_T/σ tested, for C_T/σ greater than 0.077 the force/thrust ratio is slightly positive (upload). Since the rotated part of the wing is immersed in the rotor wake, the flow field is characterized by a non–negligible swirl component. Due to this and thanks to the rotor sense of rotation (counterclockwise), the wing sections have a negative angle of attack with respect to the flow impinging on it. Thereby, the F_z^w component of the aerodynamic force which raises on the wing is pointed upward. However, in the tilted configuration the F_z^w component is not the highest component of the aerodynamic force. In fact, the longitudinal force F_x^w, as shown in Figure 8 as a fraction of the rotor thrust, is higher than F_z^w and it is always positive. For C_T/σ higher than 0.02 the longitudinal force/thrust ratio is about 4.5 %. In Figure 8 also the longitudinal force acting on the untilted wing is reported. In this case, the force/thrust ratio is always negative and less than 0.4 % for all C_T/σ.

Both for the untilted and tilted configuration, steady CFD calculations have been performed on the half–model. The rotor has been reproduced by means of an actuator disk model embedded in the code (for the details of the calculations see Ref. [7]). Numerical calculations have performed for the hover flight condition at $C_T/\sigma = 0.117$ but, due to limitations on the hydraulic motor power, the maximum value of C_T/σ tested during the experimental campaign was slightly lower ($C_T/\sigma = 0.019$). Nevertheless, the force/thrust ratio predicted by numerical calculations for both configurations is very similar to the measured values. In the tilted case however, the CFD code predicts a negative value of the force/thrust ratio while in the experiments positive values were measured. This difference is a consequence of the actuator disk model, which is unable to reproduce the swirl effect due to the rotor rotation.

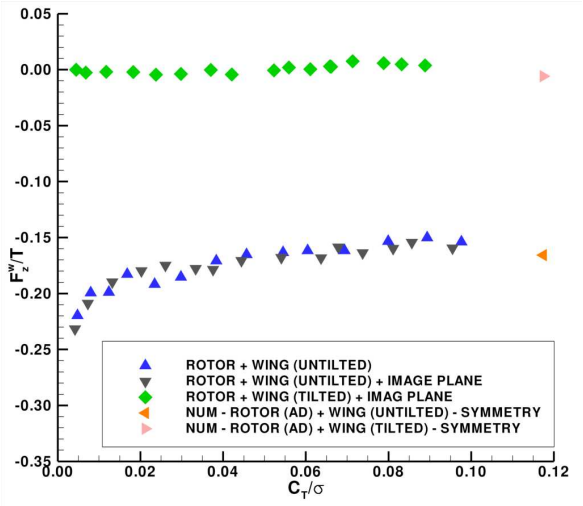

Figure 7: Wing vertical load as function of C_T/σ for the half–model tiltrotor.

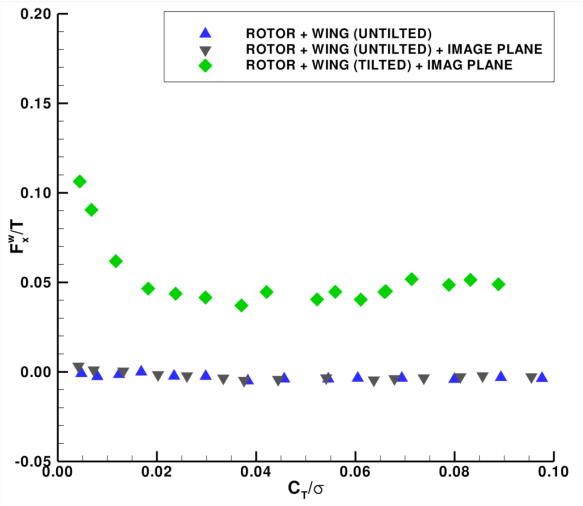

Figure 8: Wing longitudinal load as function of C_T/σ for the half–model tiltrotor.

3.4 PIV measurements

In the present work, the main goal of the PIV measurements on the flow field around the tiltwing half–model was to investigate the position of the rotor tip vortex which impinges on the lower surface of the external part of the wing. Only the tilted configuration in hover flight condition was studied and only a measurement plane was considered. The PIV test rig is reported in Figure 9. The measurement plane was parallel to the tilted wing chord ad is located 15 mm far from the wing lower surface in its maximum thickness point. The measurement area was composed by two measurement windows in the chord direction with a small overlapping band between them. All the PIV measurements were acquired at a reduced rotational speed of the rotor,

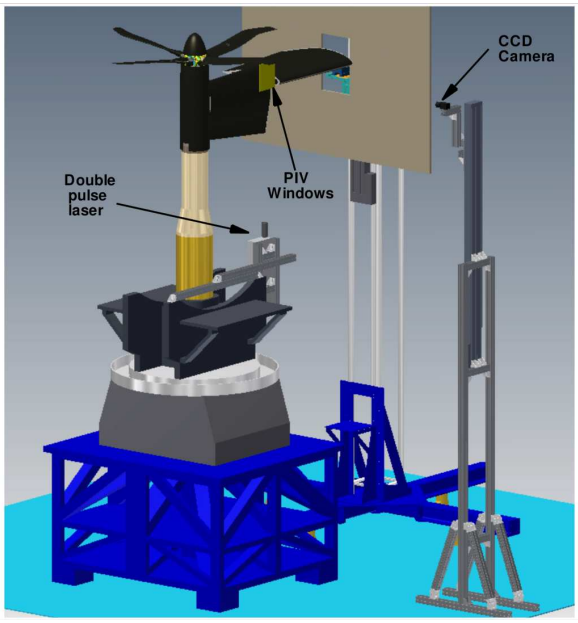

Figure 9: Particle image velocimetry setup.

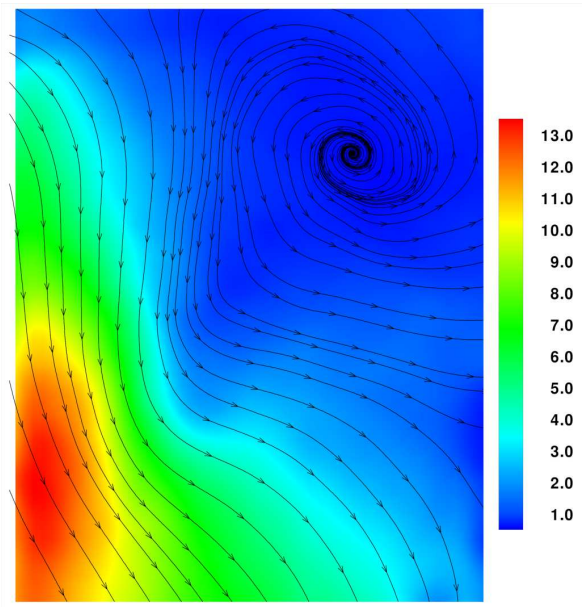

Figure 10: Particle image velocimetry results: velocity magnitude contours and two–dimensional streamline patterns.

that was 850 rpm, due to a frequency limitation on the PIV system. Before to start with the PIV measurements, a few PIV surveys were carried out to find the master blade azimuth position (Ψ) on which the rotor tip vortex strikes on the wing surface. Taking the blade azimuth position measured in the direction of rotor rotation starting from the wing axis, the phase angle results $\Psi = 28°$. Once the blade position was defined, PIV surveys were done and the velocity flow fields were phase averaged over 100 image pairs. Figure 10 shows the result of the PIV measurements in which velocity magnitude contours are illustrated. In the same image, the two–dimensional streamline patterns related to in-plane velocity are represented.

4 Conclusions

To study the aerodynamic interference between wing and rotor in a tiltwing aircraft, a research acrivity has been started at Dipartimento di Scienze e Tecnologie Aerospaziali (DAST) of Politecnico of Milano. An aircraft of the same kind of ERICA has been defined and a 0.25 scale tiltwing experimental half–model for hover tests has been manufactured. Both the aerodynamic influence of the wing on the rotor performance and the effects of the rotor wake on the wing have been investigated using tests data. A good agreement with CFD calculation has been found in terms of FM for the isolated rotor. When the wing was placed under the rotor, the FM is increased for both untilted and tilted configurations. The untilted configuration gives the maximum value of FM (0.76) and shows a negative value of vertial aerodynamic force on the wing (about 15.6 % of the rotor thrust). However, in the tilted configuration the FM increase is lower than in the previous case (0.73), but the vertical aerodynamic force measured on the wing is positive and very low (less than 0.8 %). In this configuration a non–negligible positive longitudinal force (about 4.5 % of the rotor thrust) has been observed. The effects due to the image plane on the model have been investigated. While no significant effects have been found for the tilted configuration, with the wing untilted a little decrease in rotor performance have been noted when the image plane has been installed. Particle–image velocimetry (PIV) system developed in–house has been used to identify the position of the rotor tip vortex impinging on the tilted wing with two–dimensional images of the flow field.

References

[1] McVeigh, M. A., "The V–22 Tiltrotor Large–Scale Rotor Performance/Wing Download Test and Comparison With Theory," *Vertica*, Vol. 10, No. 3/4, 1986, pp. 281–297.

[2] Felker, F., "Wing Download Results from a Test of a 0.658-Scale V–22 Rotor and Wing," *Journal of the American Helicopter Society*, October 1992, pp. 58–63.

[3] Felker, F. and Light, J. S., "Aerodynamic Interactions Between a Rotor and Wing in Hover," *Journal of the American Helicopter Society*, April 1988, pp. 53–61.

[4] Darabi, A., Stalker, A., McVeigh, M., and Wygnanski, I., "The Rotor Wake Above a Tiltrotor Airplane–Model in Hover," *AIAA*, 33rd AIAA Fluid Dynamics Conference, Orlando, Florida, USA, 23–26 June 2003.

[5] McVeigh, M., Grauer, W., and Paisley, D., "Rotor/Airframe Interaction On Tiltrotor Aircraft," *Journal of American Helicopter Society*, Vol. 35, No. 3, July 1990, pp. 43–51.

[6] Polak, D., Rehm, W., and George, A., "Effects of an Image Plane on the Tiltrotor Fountain Flow," *Journal of American Helicopter Society*, Vol. 45, No. 2, April 2000, pp. 90–96.

[7] Droandi, G., Gibertini, G., and Biava, M., "Wing–Rotor Aerodynamic Interaction in Tiltrotor Aircraft," 38^{th} European Rotorcraft Forum, Amsterdam, The Netherlands, 4–7 September 2012.

[8] Alli, P., Nannoni, F., and Cicalè, M., "ERICA: The european tiltrotor design and critical technology projects," *AIAA/ICAS*, International Air and Space Symposium and Exposition: The Next 100 Years, Day-ton, Ohio, USA, 14–17 July 2005.

[9] Gibertini, G., Auteri, F., Campanardi, G., Macchi, C., Zanotti, A., and Stabellini, A., "Wind tunnel tests of a tilt–rotor aircraft," *Aeronautical Journal*, Vol. 115, No. 1167, May 2011, pp. 315–322.

[10] Lefebvre, T., Beaumier, P., Canard-Caruana, S., Pisoni, A., Pagano, A., Sorrentino, A., der Wall, B. V., Yin, J., Arzoumanian, C., Voutsinas, S., and Hermans, C., "Aerodynamic and aero-acoustic optimization of modern tilt-rotor blades within the ADYN project," *ECCOMAS*, 4th European Congress on Computational Methods in Applied Sciences and Engineering, Jyväskylä, Finlande, 24–28 July 2004.

[11] Zanotti, A. and Gibertini, G., "Experimental investigation of the dynamic stall phenomenon on a NACA 23012 oscillating airfoil," *Proc of IMechE, Part G: Journal of Aerospace Engineering*, In press.

[12] Zanotti, A., *Retreating blade dynamic stall*, Ph.D. thesis, Politecnico di Milano, 2012.

[13] PIVTEC, "PIVview 2C version 3.0. User manual," `www.pivtec.com`, January 2009.

[14] Biava, M., Boniface, J.-C., and Vigevano, L., "Influence of wind–tunnel walls in helicopter aerodynamics predictions," 31^{st} European Rotorcraft Forum, Florence, Italy, 13–15 September 2005.

[15] Biava, M., *RANS computations of rotor/fuselage unsteady interactional aerodynamics*, Ph.D. thesis, Politecnico di Milano, 2007.